

## Electronic Supplementary Information

# Macroscopical Monolayer Films of Ordered Arrays of Gold Nanoparticles as SERS Substrates for *in-situ* Quantitative Detection in Aqueous Solutions

Lixiang Xing,<sup>a</sup> Cui Wang,<sup>a</sup> Yi Cao,<sup>a</sup> Jihui Zhang,<sup>b</sup> and Haibing Xia<sup>\*a</sup>

<sup>a</sup> State Key Laboratory of Crystal Materials, Shandong University, Jinan, 250100, P. R. China.

E-mail: hbxia@sdu.edu.cn

<sup>b</sup> School of Materials Science & Engineering, Qilu University of Technology (Shandong Academy of Sciences), Jinan, 250353, P. R. China.

**Figure S1.** Zeta potentials of citrate-stabilized Au NPs (red curve) before traditional phase transfer and OLA-Au NPs (green curve) after traditional phase transfer.

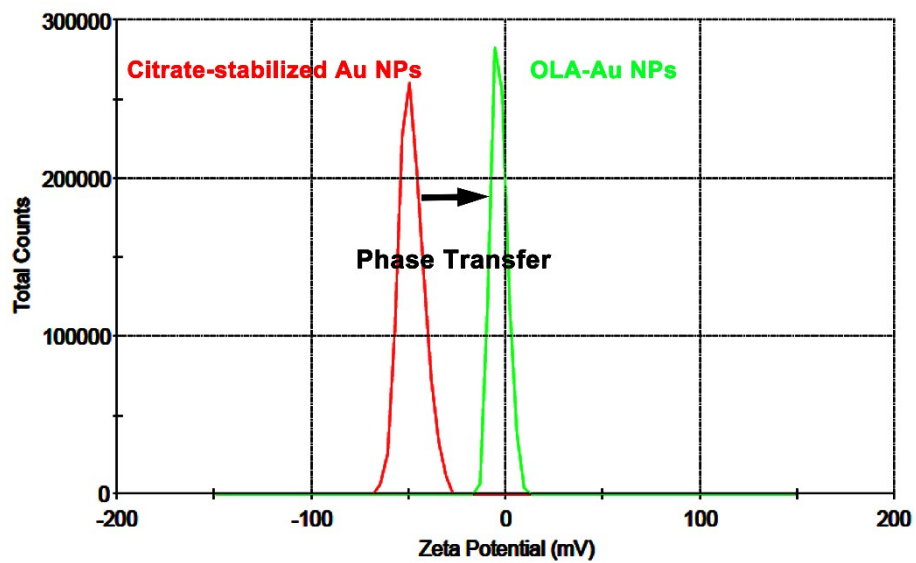


**Figure S2.** TEM image (a) and extinction spectrum (b) of citrate-stabilized Au NPs in the aqueous solution.

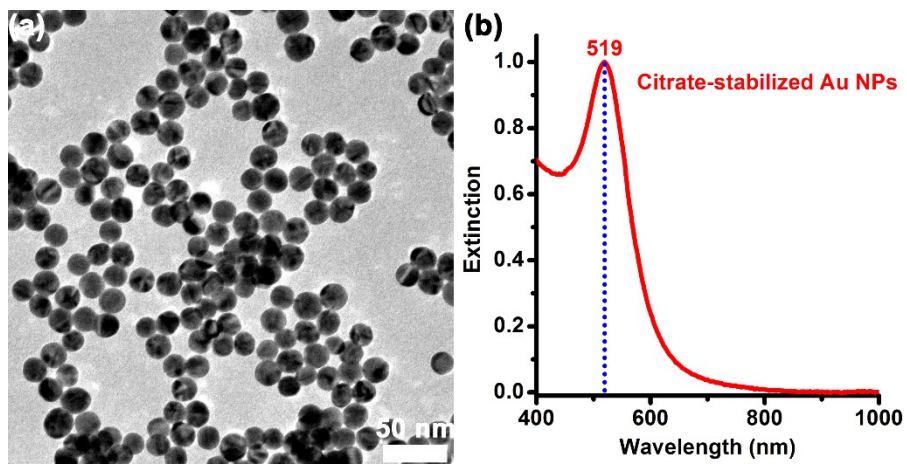


**Figure S3.** TEM image (a) and extinction spectrum (b) of OLA-Au NPs in the toluene phase.

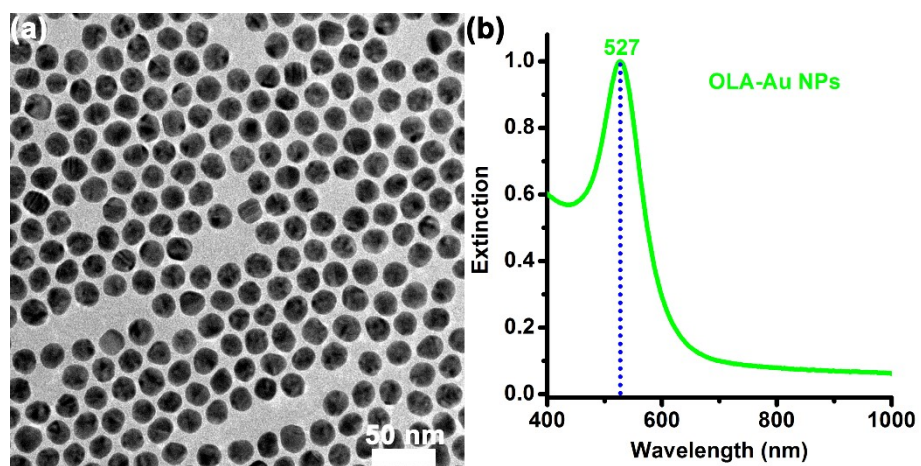


**Figure S4.** Schematic representation for the preparation procedure of the MMF-OA-Au NPs. (a) Pure DEG phase, (b) the homogenous DEG solution containing a water volume fraction of 10%, (c) direct addition of OLA-Au NPs in the toluene phase containing on the surface of the homogenous DEG solution, and (d) formation of MMF-OA-Au NPs on the surface of the homogenous DEG solution after slow toluene evaporation of about 12 h.

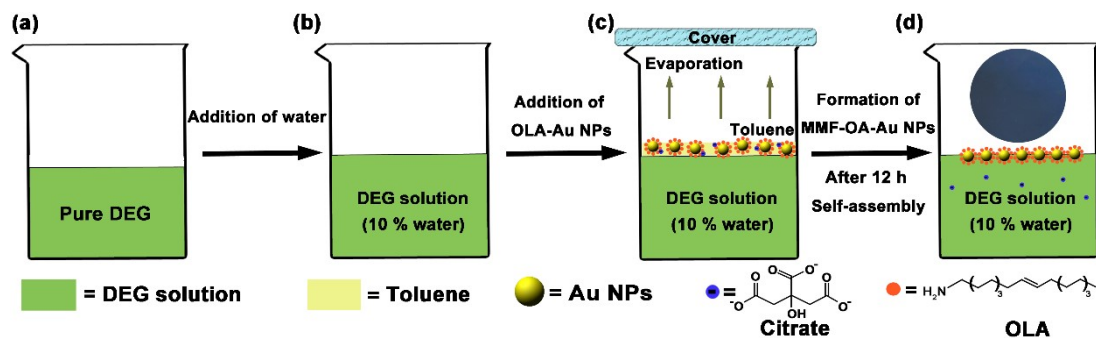
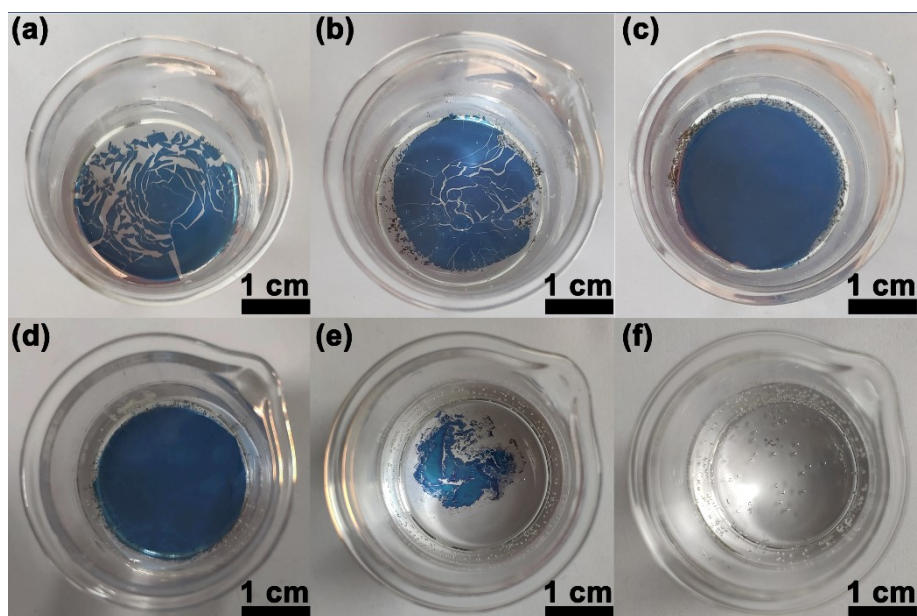


**Figure S5.** Digital photos of a series of films formed on the surfaces of homogenous DEG solutions containing different water volume fractions by using the same OLA-Au NPs in the toluene phase. The volume fractions of water are 0 % (a), 5 % (b), 10 % (c), 25 % (d), 50 % (e), and 100 % (f), respectively. The total volumes of all of homogenous DEG solutions were fixed to 20 mL.



When the water volume fraction in the DEG solutions is below 10 %, the intact monolayered films cannot be formed on the surfaces of the DEG solutions. And the films are composed of many pieces of small broken films (**Figure S5a** and **S5b**).

When the water volume fractions in the DEG solutions is between 10 % and 25 %, the intact monolayered film can be formed on the surfaces of the DEG solutions. And there are no obvious cracks in the films (**Figure S5c** and **S5d**).

When the water volume fractions in the DEG solutions is bigger than 25 % (less than 100 %), the intact monolayered film cannot be formed, which is composed of many pieces of small broken films. And it seems that the film is composed of aggregates of Au NPs (**Figure S5e**).

When pure water is used, there is no any film formed on the surface due to larger surface pressure (**Figure S5f**).

**Figure S6.** Typical extinction spectra of the film on PDMS substrate measured at five different positions. The film was formed on the surface of pure DEG phase (**Figure S5a**) and then transferred onto PDMS substrate. The inset is the corresponding optical photo of the resulting film.

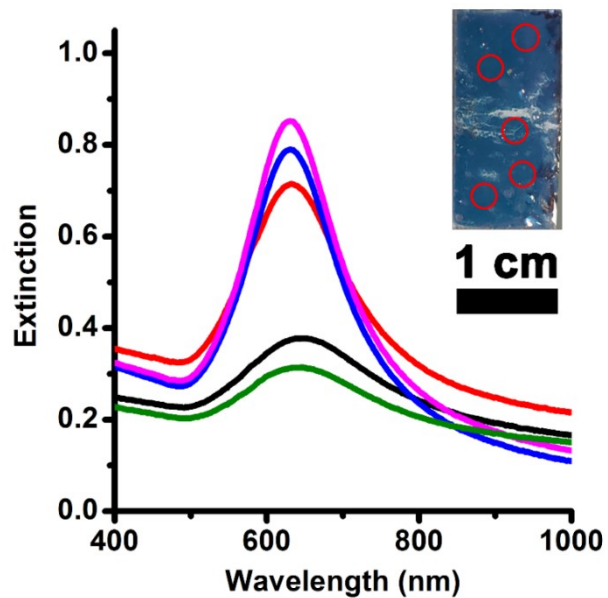
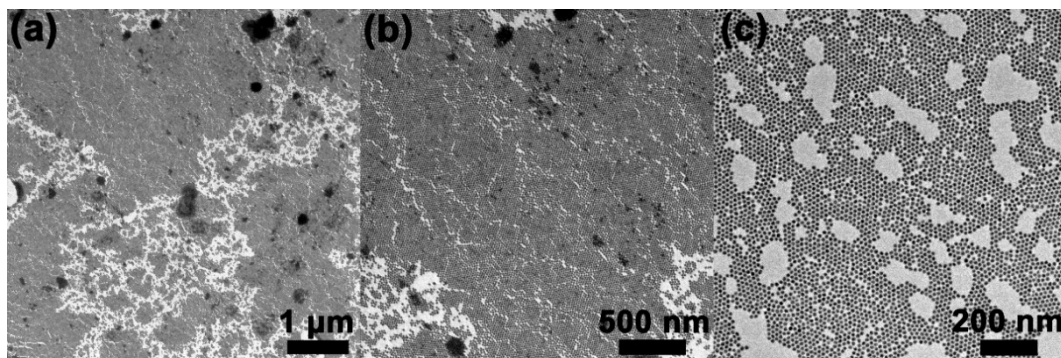
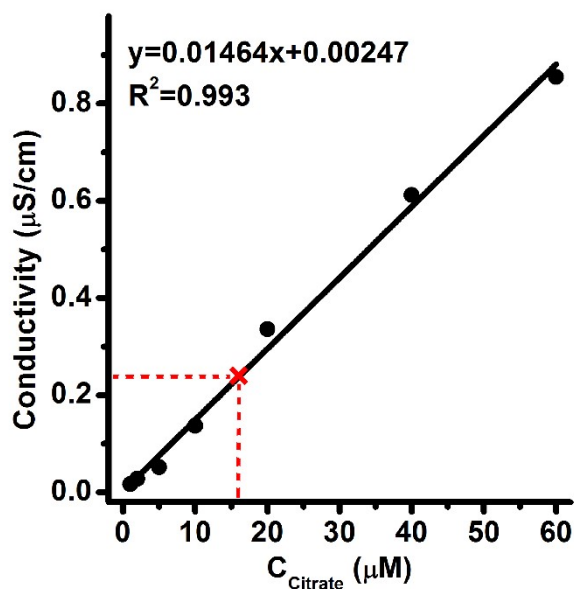


**Figure S7.** Typical TEM images of the resulting film formed on the surface of pure DEG phase (**Figure S5a**), which were investigated by transferring it onto copper grids.



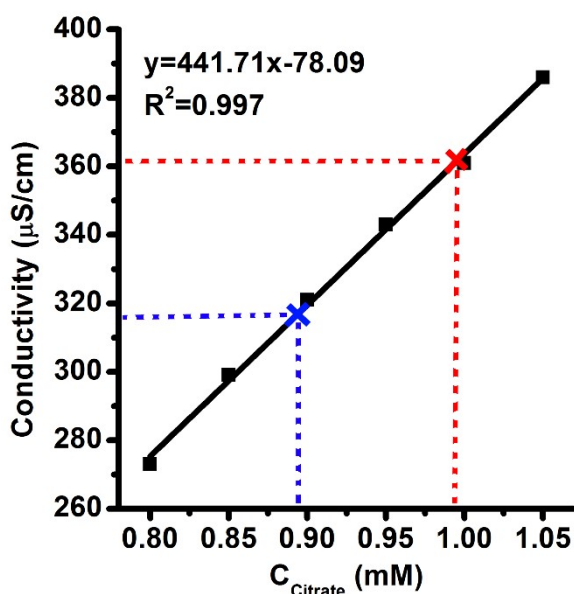
The resulting film formed on the surface of pure DEG phase was investigated by its TEM images. At low magnification TEM images (**Figure S7a and S7b**), many cracks and black dots (agglomerates of Au NPs) are observed in the film. Obviously, the whole film has been broken into many pieces of small films. At a high magnification TEM image of one complete piece of small films, there are many voids are observed (**Figure S7c**). The result demonstrates that the OLA-Au NPs obtained by traditional phase transfer cannot be directly used to prepare high quality MMF-OA-Au NPs by self-assembly at toluene-DEG interfaces.

**Figure S8.** Established standard curve of the actual conductivity of the DEG solution (containing a water volume fraction of 10 %) versus the citrate concentration in the range of 1 to 60  $\mu\text{M}$  on the basis of the data from **Table S3**.



The actual conductivity of the final DEG solution after the self-assembly process (**Table S2**) is 0.236  $\mu\text{S/cm}$  (indicated by the red crosser). On the basis of its actual conductivity (0.236  $\mu\text{S/cm}$ ) and the established standard curve (**Figure S8**), the actual concentration of citrate ions in the final DEG solution after the self-assembly process is calculated to be 15.95  $\mu\text{M}$  (indicated by the red crosser). Since the total volume of the DEG solution is 20 mL, the total amount of citrate ions in the final DEG solution after the self-assembly process is about  $3.19 \times 10^{-7}$  mol.

**Figure S9.** Established standard curve of the actual conductivity of the water versus the citrate concentration in the range of 0.80 to 1.05 mM on the basis of the data from **Table S4**.



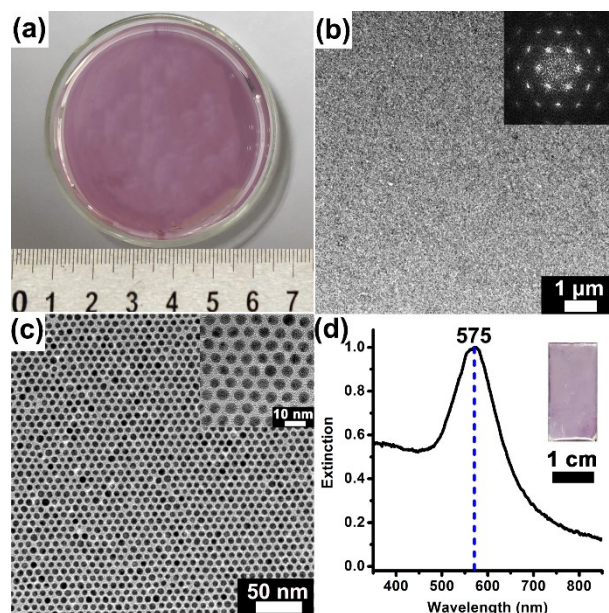
(1) The actual conductivity of the aqueous solution of the citrate-stabilized Au NPs before traditional phase transfer (**Table S5**) is 361  $\mu\text{S}/\text{cm}$  (indicated by the red crosser). On the basis of its actual conductivity (361  $\mu\text{S}/\text{cm}$ ) and the established standard curve (**Figure S9**), the actual concentration of citrate ions of the aqueous solution before traditional phase transfer is calculated to be 0.994 mM (indicated by the red crosser).

(2) The actual conductivity of the aqueous solution of the citrate-stabilized Au NPs after traditional phase transfer (**Table S5**) is 316  $\mu\text{S}/\text{cm}$  (indicated by the blue crosser). On the basis of its actual conductivity (316  $\mu\text{S}/\text{cm}$ ) and the established standard curve (**Figure S9**), the actual concentration of citrate ions of the aqueous solution after traditional phase transfer is calculated to be 0.892 mM (indicated by the blue crosser).

(3) Accordingly, the change of the actual concentration of citrate ions of the aqueous solution before (0.994 mM) and after traditional phase transfer (0.892 mM) is about 0.102 mM. And the actual concentration of citrate ions remaining in the toluene phase of OLA-Au NPs after traditional phase transfer is calculated to be 0.510 mM, since the volume ratio of the aqueous solution of citrate-stabilized Au NPs to the toluene phase is 5:1. Thus, the total amount of citrate ions remaining in the toluene phase of OLA-Au NPs after phase transfer is calculated to be about  $3.32 \times 10^{-7}$  mol based on the total volume of the toluene phase of OLA-Au NPs (0.65 mL).

(4) Since the total amount of citrate ions in the final DEG solution after the self-assembly process and that in the toluene phase of OLA-Au NPs are  $3.19 \times 10^{-7}$  mol and  $3.32 \times 10^{-7}$  mol, more than 95 % of the residual citrate ions in the toluene solution of OLA-Au NPs are transferred into the DEG solution after the self-assembly process.

**Figure S10.** (a) Digital photo of MMF-OA-Au NPs (6 nm) on the surface of the DEG solution, low (b) and high (c) magnification TEM images of MMF-OA-Au NPs (6 nm) on copper grids, and extinction spectrum (d) of MMF-OA-Au NP@PDMS (6 nm). Insets in (b), (c) and (d) are the fast Fourier transform (FFT) pattern, the typical feature of hexagonal close-packed arrangement, and the digital photo of MMF-OA-Au NP@PDMS (6 nm), respectively.



Quasi-spherical 6 nm Au NPs were firstly prepared according to the protocol reported in our previous work.<sup>1</sup> Then, OLA-Au NPs (6 nm) were obtained by the same treatment of phase transfer process. Lastly, MMF-OA-Au NPs (6 nm) were fabricated through our method (**Figure S10**).

**Figure S10a** is the digital photo of the resulting MMF-OA-Au NPs (6 nm) self-assembled on the DEG surface with an area of up to 30 cm<sup>2</sup>. And it shows a light purple color. There are hardly small black dots (agglomerates of Au NPs) existed in the MMF, indicating high quality of the as-prepared MMFs. As shown in their low magnification TEM image (**Figure S10b**), the whole MMF is indeed composed of ordered arrays of 6 nm Au NPs, in which no obvious voids, cracks and accumulations are observed. The inset in **Figure S10b** is the fast Fourier transform (FFT) pattern of the selected area in the TEM image, which shows a clear hexagonal-like array. Moreover, the hexagonal close-packed (hcp) arrangement of 6 nm Au NPs in the MMF is further revealed by HRTEM image (**Figure S10c**). All of the results confirm that the periodic and orderly arrangement of 6 nm Au NPs in the as-prepared MMF. **Figure S10d** is the extinction spectrum of MMF-OA-Au NP@PDMS and the inset is their corresponding optical photo. The peak position of the surface plasmon resonance (SPR) band of MMF-OA-Au NP@PDMS is near 575 nm. And its SPR band is relatively symmetrical and has a narrow half-width, which further indicates the ordered arrangement of 6 nm Au NPs in the resulting MMF.

**Figure S11.** Optical photo (a) of *in-situ* SERS detection in aqueous solution by using MMF-OA-Au NP@PDMS as SERS substrates with  $\times 50$  long distance objective. Optical photos (b and c) are the corresponding photos of the cell from side view and top view.

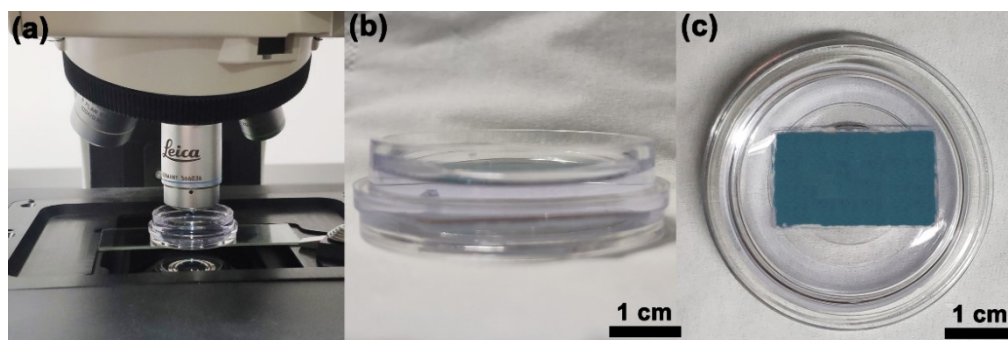
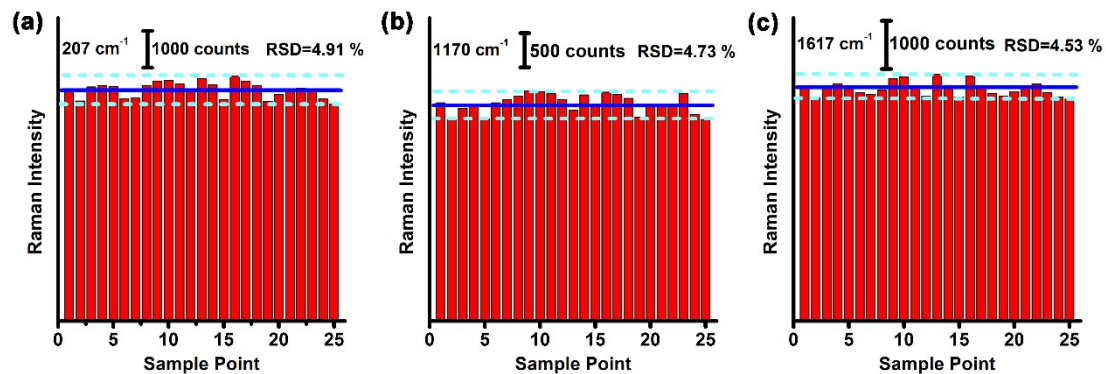


**Figure S12.** The histograms of the intensities of the corresponding Raman peaks at about 207  $\text{cm}^{-1}$  (a), 1170  $\text{cm}^{-1}$  (b) and 1617  $\text{cm}^{-1}$  (c) in SERS spectra of CV probes (**Figure 3b**). The wavelength and power of the laser are 633 nm and 0.0425 mW, respectively. And the acquisition time is 10 s.



The RSDs in the intensity of the Raman peaks at about 207  $\text{cm}^{-1}$  (a), 1170  $\text{cm}^{-1}$  (b) and 1617  $\text{cm}^{-1}$  (c) in SERS spectra of CV probes are 4.91 %, 4.73 % and 4.53 %, respectively.

**Figure S13.** Typical SERS spectra of different concentrations (from  $10^{-10}$  to  $10^{-6}$  M) of CV probes in aqueous solutions. The wavelength and power of the laser are 633 nm and 0.0425 mW, respectively. And the acquisition time is 10 s.

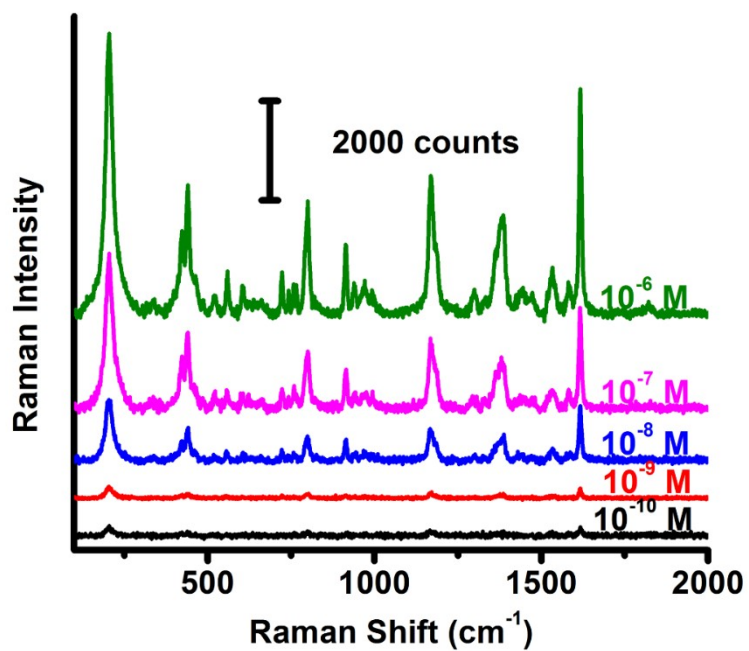


**Figure S14.** Linear relationships between the intensities of the Raman peaks of CV probes and the CV concentrations in the logarithm: 207  $\text{cm}^{-1}$  (a, blue line) and 1170  $\text{cm}^{-1}$  (b, red line). The error bars in the peak intensity for each concentration of CV probes are determined according to the standard errors from five parallel SERS spectra. The wavelength and power of the laser are 633 nm and 0.0425 mW, respectively. And the acquisition time is 10 s.

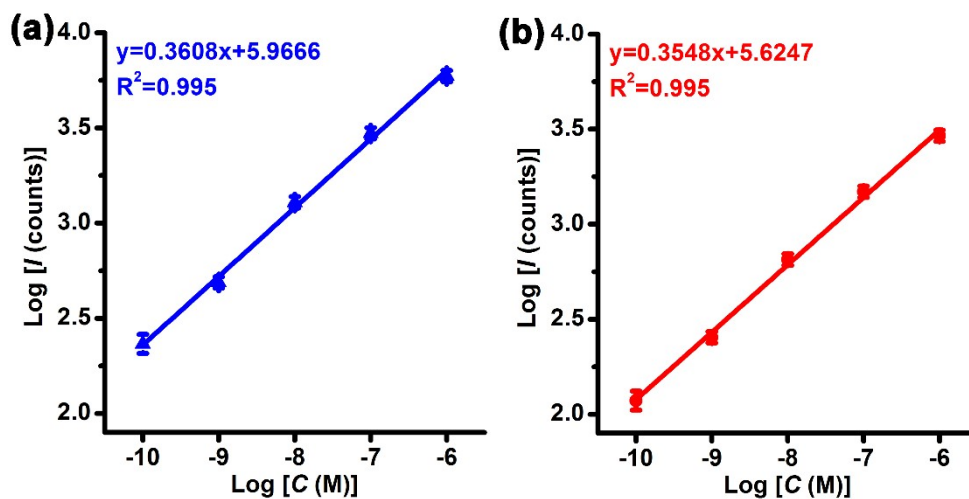
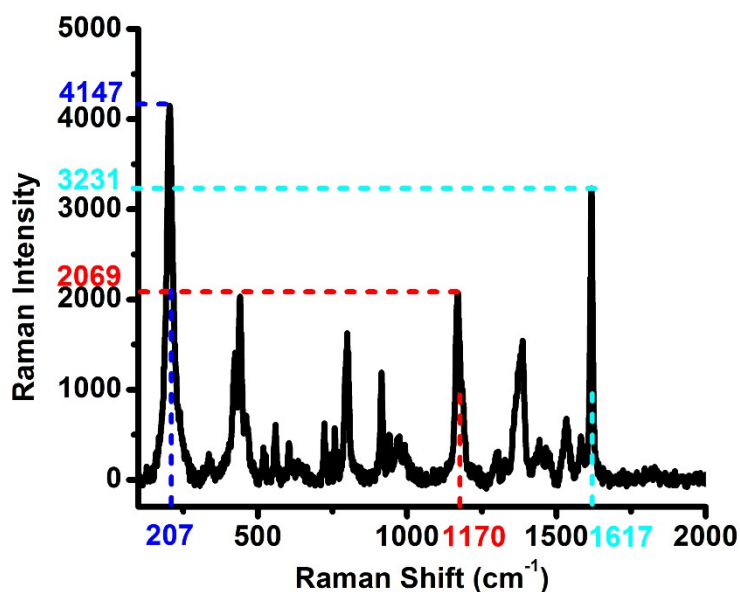


**Figure S15.** SERS spectrum of CV probes ( $3 \times 10^{-7}$  M) in the aqueous solution. The wavelength and power of the laser are 633 nm and 0.0425 mW, respectively. And the acquisition time is 10 s.



On the basis of the intensity (3231) at  $1617 \text{ cm}^{-1}$  in the SERS spectrum of the standard sample (**Figure S15**) and the established standard work curve (**Figure 4a**), the concentration of the standard sample is calculated to be  $2.98 \times 10^{-7}$  M, which is almost equal to the actual one. Similarly, on the basis of the intensities (4147 and 2069) at  $207 \text{ cm}^{-1}$  and  $1170 \text{ cm}^{-1}$  in the SERS spectrum of the standard sample (**Figure S15**) and the corresponding established standard work curves (**Figure S14a** and **S14b**), the concentrations of the standard sample are calculated to be  $3.09 \times 10^{-7}$  and  $3.11 \times 10^{-7}$  M, respectively. The obtained concentrations are a little higher than the actual one. Thus, the best standard work curve is the one based on the intensity at  $1617 \text{ cm}^{-1}$  in the SERS spectrum and the CV concentration in the logarithm.

**Figure S16.** SERS spectra of CV probes ( $10^{-6}$  M) adsorbed on the MMF-OA-Au NP@PDMS before (a, black curve) and after (b, red curve) the heating-treatment at a proper temperature of  $160$  °C for the removal of CV probes. SERS spectrum (c, blue curve) of CV probes ( $10^{-6}$  M) re-adsorbed on the MMF-OA-Au NP@PDMS. The wavelength and power of the laser are  $633$  nm and  $0.0425$  mW, respectively. And the acquisition time is  $10$  s.

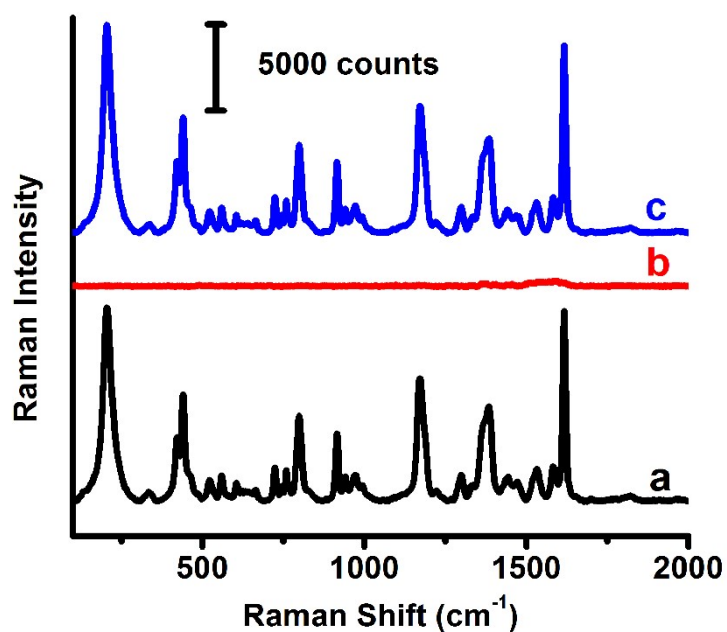
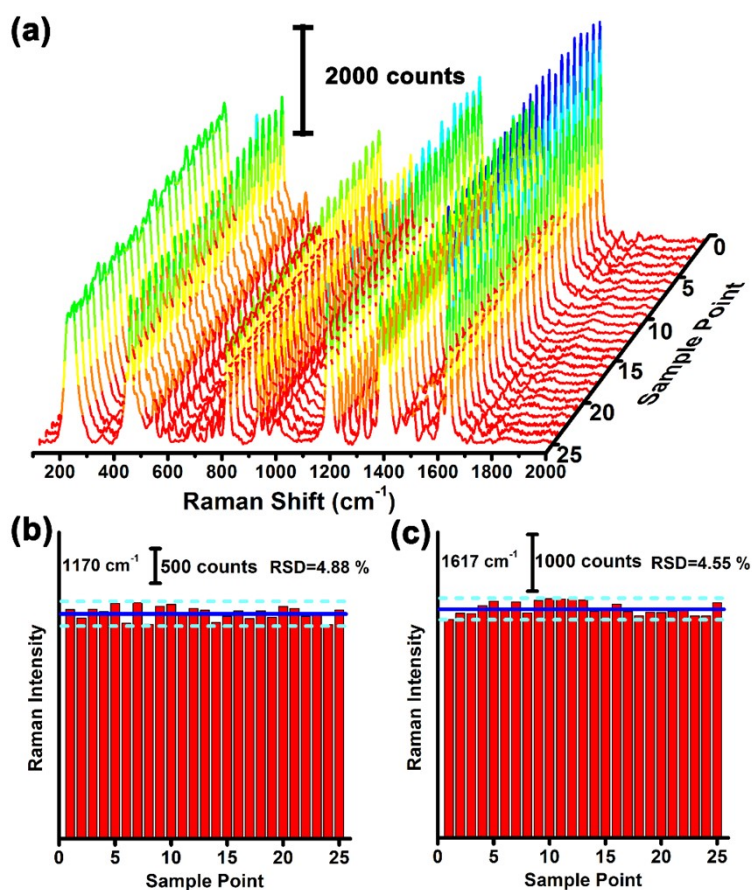
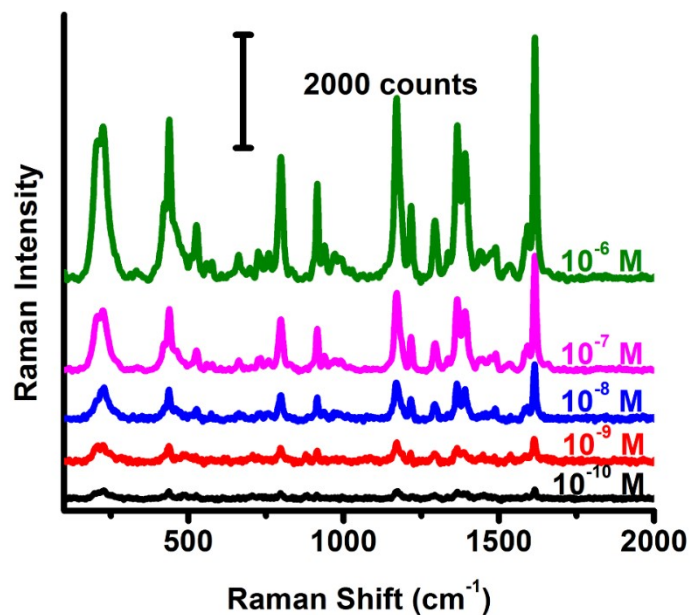


**Figure S17.** SERS spectra (a) of MG probes ( $10^{-6}$  M) in the aqueous solution, which were measured on 25 different positions in a square frame of  $25\ \mu\text{m} \times 25\ \mu\text{m}$  with point-to-point distance of  $5\ \mu\text{m}$ . The histograms of the intensities of the corresponding Raman peaks at about  $1170\ \text{cm}^{-1}$  (b) and  $1617\ \text{cm}^{-1}$  (c). The wavelength and power of the laser are  $633\ \text{nm}$  and  $0.0425\ \text{mW}$ , respectively. And the acquisition time is  $10\ \text{s}$ .



As shown in **Figure S17a**, the uniformity in their SERS signals is observed. And the RSDs in the intensity of the Raman peaks at about  $1170\ \text{cm}^{-1}$  (**Figure S17b**) and  $1617\ \text{cm}^{-1}$  (**Figure S17c**) in SERS spectra of MG probes are 4.88 % and 4.55 %, respectively. The result proves that the as-prepared MMF-OA-Au NP@PDMS as SERS substrates can also be used for *in-situ* detection in the MG solution.

**Figure S18.** Typical SERS spectra of different concentrations (from  $10^{-10}$  to  $10^{-6}$  M) of MG probes in aqueous solutions. The wavelength and power of the laser are 633 nm and 0.0425 mW, respectively. And the acquisition time is 10 s.



Since their main Raman characteristic peaks still can be observed at the concentration of  $10^{-10}$  M and the signal-to-noise ratio (S/N) at the concentration is greater than 3 (**Figure S18**), the limit of detection (LOD) of MMF-OA-Au NP@PDMS for MG probes in aqueous solutions is determined to be  $10^{-10}$  M.

**Figure S19.** Linear relationships between the intensities of the Raman peak at 1170  $\text{cm}^{-1}$  of MG probes and the corresponding MG concentrations in the logarithm. The error bars at the peak intensity for each concentration are determined according to the standard errors from five parallel SERS spectra. The wavelength and power of the laser are 633 nm and 0.0425 mW, respectively. And the acquisition time is 10 s.

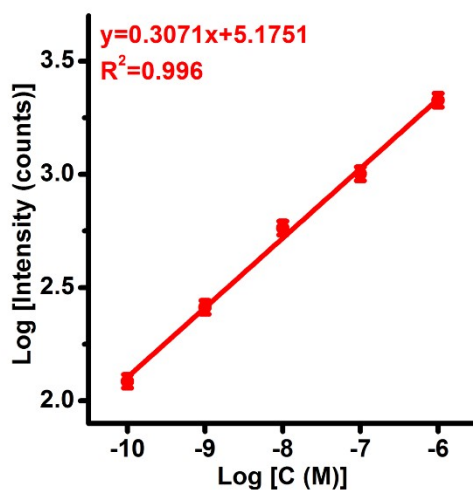
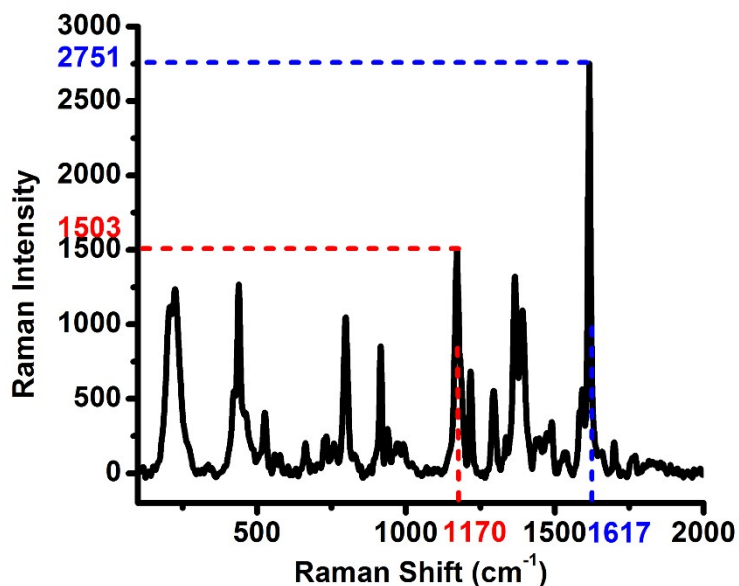


**Figure S20.** SERS spectrum of MG probes ( $3 \times 10^{-7}$  M) in the aqueous solution. The wavelength and power of the laser are 633 nm and 0.0425 mW, respectively. And the acquisition time is 10 s.



On the basis of the intensity (2751) at  $1617 \text{ cm}^{-1}$  in the SERS spectrum of the standard sample (**Figure S20**) and the established standard work curve (**Figure 4b**), the concentration of the standard sample is calculated to be  $3.02 \times 10^{-7}$  M, which is almost equal to the actual one. Similarly, on the basis of the intensity (1503) at  $1170 \text{ cm}^{-1}$  in the SERS spectrum of the standard sample (**Figure S20**) and the corresponding established standard work curve (**Figure S19**), the concentration of the standard sample is calculated to be  $3.12 \times 10^{-7}$  M. The obtained concentration is a little higher than the actual one. Thus, the best standard work curve is the one based on the intensity at  $1617 \text{ cm}^{-1}$  in the SERS spectrum and the MG concentration in the logarithm.

**Figure S21.** SERS spectra of MMF-OA-Au NP@PDMS without any functionalization measured in aqueous solutions with pH values ranging from pH 3 to 10. The wavelength and power of the laser are 633 nm and 0.0425 mW, respectively. And the acquisition time is 10 s.

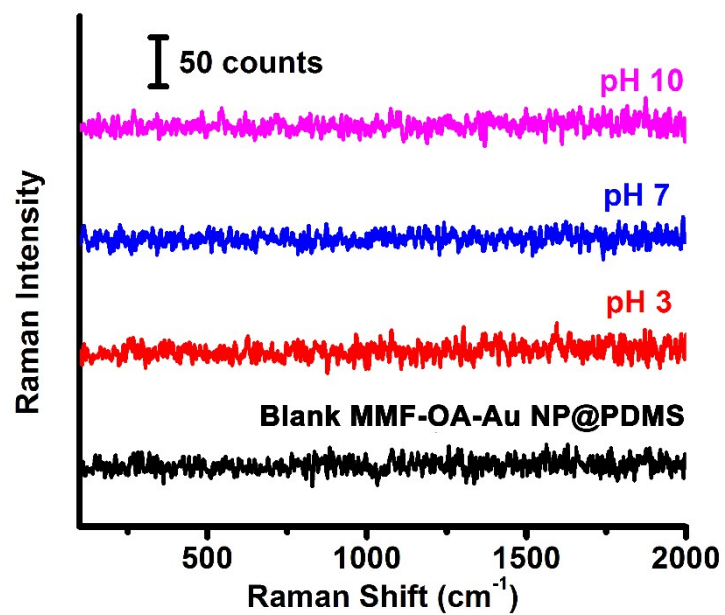
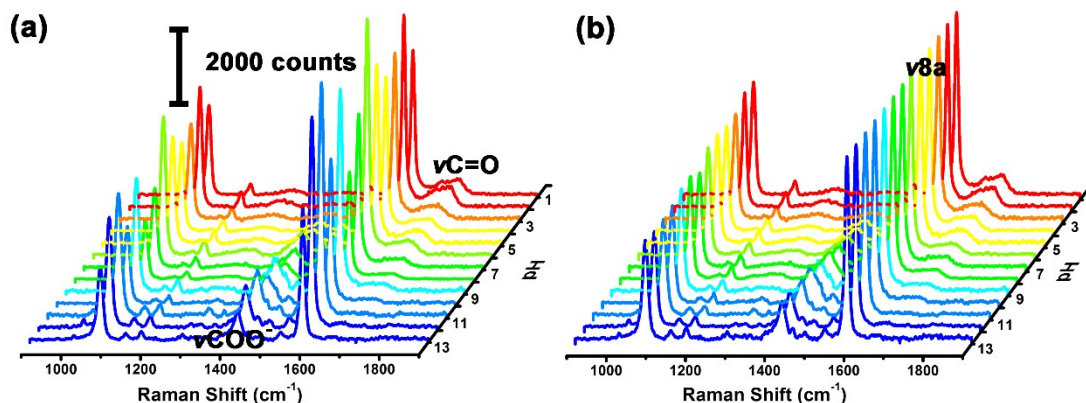


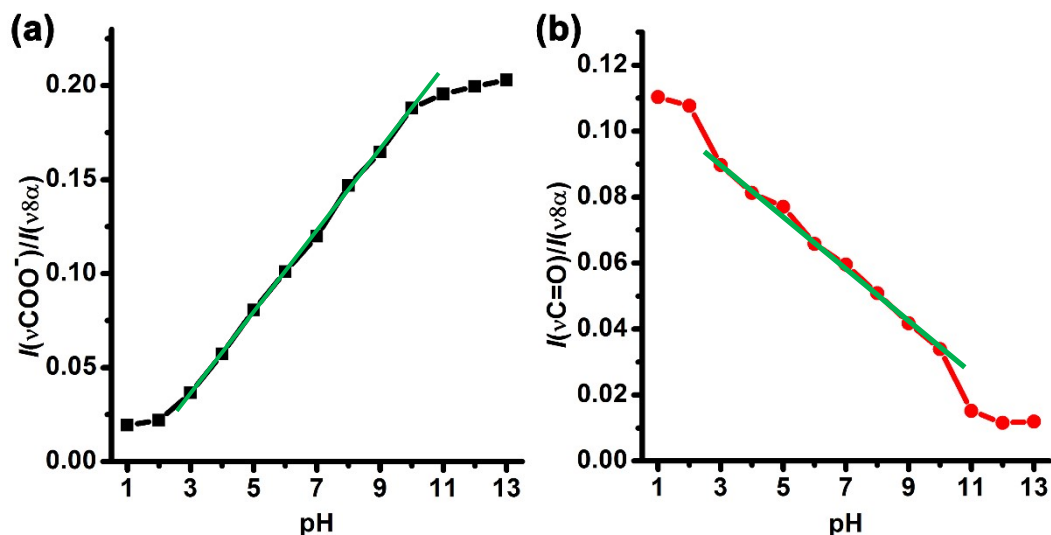
**Figure S22.** (a) Original SERS spectra of DOA-Au NP@PDMS functionalized with 4-MBA molecules measured in aqueous solutions with pH values ranging from 1 to 13. (b) Normalized SERS spectra by using the intensity of the peak of  $\nu_{8a}$  as the reference. The wavelength and power of the laser are 633 nm and 0.0425 mW, respectively. And the acquisition time is 10 s.



As shown in **Figure S22a**, there are two important Raman characteristic peaks at about 1420 and 1690  $\text{cm}^{-1}$  in the SERS spectra of 4-MBA molecules on the DOA-Au NP@PDMS. These two Raman peaks are originated from the stretching modes of the  $\text{COO}^-$  group ( $\nu_{\text{COO}^-}$ ) and the C=O group ( $\nu_{\text{C=O}}$ ) of 4-MBA molecules, respectively. The variation in their intensity can reflect the variation of the pH value of an aqueous solution. However, their original intensities are obviously fluctuated with pH values of aqueous solutions (ranging from 1 to 13). Thus, it is difficult to directly obtain pH values by using the intensities of either of them as the reference.

In previous works, it is always necessary to firstly normalize the obtained SERS signals of 4-MBA molecules on the DOA-Au NP@PDMS by using the intensity of the peak at about 1590  $\text{cm}^{-1}$  ( $\nu_{8a}$  aromatic ring vibration) as the reference, followed by the comparison of the intensity of the peak of  $\nu_{\text{COO}^-}$  or  $\nu_{\text{C=O}}$  with them, as shown in **Figure S22b**.

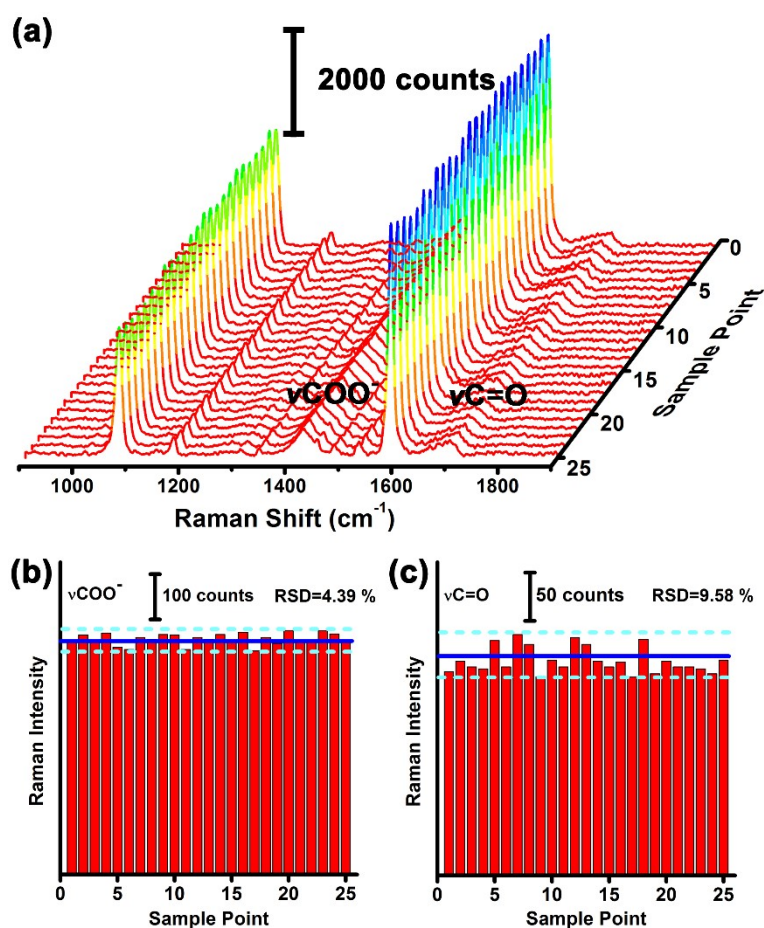
**Figure S23.** Line chart (a, black line) plotted by the pH value of the aqueous solution versus the intensity ratio of the Raman peaks of  $\nu\text{COO}^-$  to  $\nu 8a$  (**Figure S22b**). Line chart (b, red line) plotted by the pH value of the aqueous solution versus the intensity ratio of the Raman peaks of  $\nu\text{C}=\text{O}$  to  $\nu 8a$  (**Figure S22b**). The wavelength and power of the laser are 633 nm and 0.0425 mW, respectively. And the acquisition time is 10 s.



After the calibration (**Figure S22b**), the line chart of the pH values of aqueous solutions ranging from 1 to 13 with the intensity ratios of the Raman peaks of  $\nu\text{COO}^-$  to  $\nu 8a$  can be plotted (**Figure S23a**). It seems that when the pH value of the aqueous solution is in the range of 3 to 10, the intensity ratio of the Raman peaks of  $\nu\text{COO}^-$  to  $\nu 8a$  linearly increases with the increasing pH value (green line for eye guidance). As expected, the linear curve (**Figure 6c**) for the determination of the pH values of aqueous solutions can be established by using the intensity ratio of the Raman peaks of  $\nu\text{COO}^-$  to  $\nu 8a$  versus the pH value of the aqueous solution.

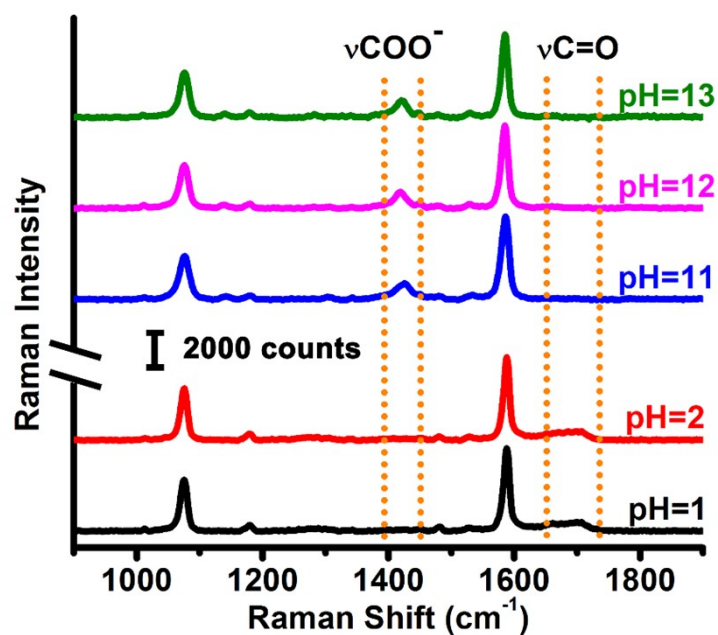
Similarly, the line chart of the pH values of aqueous solutions ranging from 1 to 13 with the intensity ratios of the Raman peaks of  $\nu\text{C}=\text{O}$  to  $\nu 8a$  is also plotted (**Figure S23b**). It seems that the linear relationship in the pH range of 3 to 10 in **Figure S23b** is worse than that in **Figure S23a**. In addition, the values of the intensity ratio of the peaks of  $\nu\text{C}=\text{O}$  to  $\nu 8a$  are rather smaller than those of  $\nu\text{COO}^-$  to  $\nu 8a$ . Thus, the linear curve (**Figure 6c**) obtained by using the intensity ratios of the Raman peaks of  $\nu\text{COO}^-$  to  $\nu 8a$  is better than that obtained by using the intensity ratios of the Raman peaks of  $\nu\text{C}=\text{O}$  to  $\nu 8a$ .

**Figure S24.** SERS spectra (a) of MMF-OA-Au NP@PDMS functionalized with 4-MBA molecules in the aqueous solution (pH=7), which were measured on 25 different positions in a square frame of  $25\ \mu\text{m} \times 25\ \mu\text{m}$  with point-to-point distance of  $5\ \mu\text{m}$ . The histograms of the intensities of the Raman peaks of  $\nu\text{COO}^-$  (b) and  $\nu\text{C}=\text{O}$  (c). The wavelength and power of the laser are 633 nm and 0.0425 mW, respectively. And the acquisition time is 10 s.



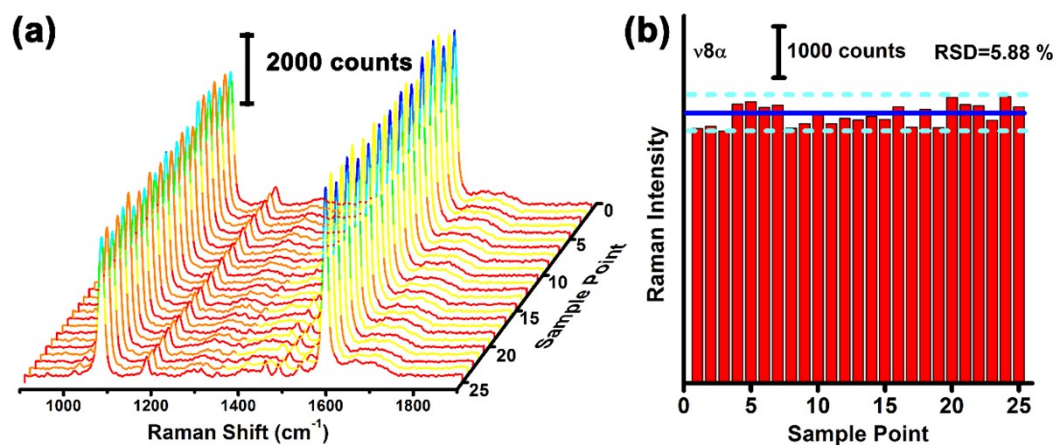
As shown in **Figure S24a**, the uniformity in their SERS signals is observed. And the RSDs in the intensity of the Raman peaks of  $\nu\text{COO}^-$  (**Figure S24b**) and  $\nu\text{C}=\text{O}$  (**Figure S24c**) in SERS spectra are 4.39 % and 9.58 %, respectively. One can clearly see that the intensities of the peak of  $\nu\text{COO}^-$  measured on 25 different positions is rather uniformity. Thus, the intensities of the peak of  $\nu\text{COO}^-$  can be directly used to determine the pH values of aqueous solutions, instead of using the intensity ratios of the Raman peaks of  $\nu\text{COO}^-$  to  $\nu\text{8a}$ .

**Figure S25.** Typical SERS spectra of MMF-OA-Au NP@PDMS functionalized with 4-MBA molecules measured in aqueous solutions with pH values of < 3 and > 10. The wavelength and power of the laser are 633 nm and 0.0425 mW, respectively. And the acquisition time is 10 s.



When the pH value of the aqueous solution is below 3, the peak of  $\nu\text{COO}^-$  does not appear at all. Meanwhile, when the pH value of the aqueous solution is above 10, the intensity of the peak of  $\nu\text{COO}^-$  changes hardly (**Figure S25**).

**Figure S26.** SERS spectra (a) of MMF-OA-Au NP@PDMS functionalized with 4-MBA molecules as SERS-based pH sensors after the storage of 20 days, which were measured on 25 different positions in a square frame of  $25\ \mu\text{m} \times 25\ \mu\text{m}$  with point-to-point distance of  $5\ \mu\text{m}$ . The histogram (b) of the intensities of the Raman peak of  $\nu_{8a}$ . The wavelength and power of the laser are 633 nm and 0.0425 mW, respectively. And the acquisition time is 10 s.



As shown in **Figure S26a**, their SERS signals in the whole film are still rather uniform. In addition, the RSD in the intensity of the Raman peak of  $\nu_{8a}$  (**Figure S26b**) in SERS spectra is still as low as 5.88 %. The result indicates that the as-prepared SERS-based pH sensors by functionalization of MMF-OA-Au NP@PDMS with 4-MBA molecules have good long-term durability.

**Table S1.** Average zeta potentials of citrate-stabilized Au NPs before traditional phase transfer and OLA-Au NPs after traditional phase transfer from five different batches.

Batch		1	2	3	4	5
Zeta Potential	Before	-49.3	-47.7	-46.9	-43.3	-48.5
[mV]	After	-2.37	-3.48	-0.93	-3.29	-1.87

**Table S2.** The relative change in the conductivity of the DEG solutions with different water volume fractions before and after the self-assembly process in **Figure S5**.

Sample image	Volume fraction of water (%)	Conductivity <sup>a</sup> ( $\mu\text{S}/\text{cm}$ )	Conductivity <sup>b</sup> ( $\mu\text{S}/\text{cm}$ )	Conductivity <sup>c</sup> ( $\mu\text{S}/\text{cm}$ )
S5a	0	0.083	0.085	0.002
S5b	5	0.092	0.158	0.066
S5c	10	0.101	0.337	0.236
S5d	25	0.267	0.739	0.472
S5e	50	0.818	1.832	1.014
S5f	100	2.010	4.690	2.680

<sup>a</sup> The original conductivities of the DEG solutions containing different water volume fractions before the self-assembly process; <sup>b</sup> the original conductivities of the DEG solutions containing different water volume fractions after the self-assembly process; <sup>c</sup> the change of the conductivities of the DEG solutions containing different water volume fractions after the self-assembly process, which were obtained by subtracting the conductivity of the corresponding DEG solutions before the self-assembly process.

**Table S3.** Establishment of standard curve of the conductivity of the DEG solution (containing a water volume fraction of 10 %) versus the citrate concentration in the range of 1 to 60  $\mu\text{M}$ .

Concentration of citrate ions ( $\mu\text{M}$ )	Conductivity <sup>a</sup> ( $\mu\text{S/cm}$ )	Conductivity <sup>b</sup> ( $\mu\text{S/cm}$ )
60	0.956	0.855
40	0.713	0.612
20	0.437	0.336
10	0.238	0.137
5	0.153	0.052
2	0.129	0.028
1	0.118	0.017

<sup>a</sup> The original conductivities of the DEG solutions containing a water volume fraction of 10 % and different concentrations of citrate; <sup>b</sup> the actual conductivities of the DEG solutions containing a water volume fraction of 10 % and different concentrations of citrate, which were obtained by subtracting the conductivity of the pure DEG solution (0.101  $\mu\text{S/cm}$ ) from the original ones.

**Table S4.** Establishment of standard curve of the conductivity of the water versus the citrate concentration in the range of 0.80 to 1.05 mM.

Concentration of citrate ions (mM)	Conductivity <sup>a</sup> ( $\mu\text{S}/\text{cm}$ )	Conductivity <sup>b</sup> ( $\mu\text{S}/\text{cm}$ )
1.05	388	386
1.00	363	361
0.95	345	343
0.90	323	321
0.85	301	299
0.80	275	273

<sup>a</sup> The original conductivities of the water containing different concentrations of citrate; <sup>b</sup> the actual conductivities of the water containing different concentrations of citrate, which were obtained by subtracting the conductivity of the water (2.010  $\mu\text{S}/\text{cm}$ ) from the original ones.

**Table S5.** The relative change in the conductivity of the aqueous solution of Au NPs before and after traditional phase transfer.

Phase transfer	Conductivity <sup>a</sup> ( $\mu\text{S}/\text{cm}$ )	Conductivity <sup>b</sup> ( $\mu\text{S}/\text{cm}$ )	Concentration of citrate ions <sup>c</sup> (mM)
Before	363	361	0.994
After	318	316	0.892
Toluene <sup>d</sup>	--	--	0.510

<sup>a</sup> The original conductivities of the aqueous solution of citrate-stabilized Au NPs before and after traditional phase transfer; <sup>b</sup> the actual conductivities of the aqueous solution of citrate-stabilized Au NPs before and after traditional phase transfer, which were obtained by subtracting the conductivity of the water (2.010  $\mu\text{S}/\text{cm}$ ) from the original ones; <sup>c</sup> the actual concentrations of citrate ions in the aqueous solution of citrate-stabilized Au NPs before and after traditional phase transfer obtained by the change of the actual conductivity in **Figure S9** and **Table S4**; <sup>d</sup> the concentration (0.51 mM) of residual citrate ions in the toluene phase of OLA-Au NPs after traditional phase transfer estimated by the change (0.102 mM) of the actual concentration of citrate ions in the aqueous solution of citrate-stabilized Au NPs before and after traditional phase transfer, according to the volume ratio (5:1) of the aqueous solution of citrate-stabilized Au NPs to the toluene phase. The actual conductivity of the toluene phase is far below the range of the instrument and cannot be obtained directly.

**Table S6.** Comparison in the performance of quantitative detection of various SERS substrates with ordered arrays.

Building block	Size of building block (nm)	Gap (nm)	Raman probe	Range of quantitative detection (M)	Limit of quantitative detection (M)	<i>In-situ</i> (Y/N)	Excitation Wavelength (nm)	References
Ag forest-like microball	1500	\	CV	$10^{-8}$ - $10^{-5}$	$10^{-8}$	N	633	[2]
Ag micro-island	4000	\	CV	$10^{-9}$ - $10^{-6}$	$10^{-9}$	N	532	[3]
Au@Ag NP	43	3	CV	$10^{-9}$ - $10^{-6}$	$10^{-9}$	N	633	[4]
Au NP	45	2-3	MG	$10^{-10}$ - $10^{-6}$	$10^{-10}$	Y	633	[5]
Ag NP	12	\	Thiram	$10^{-6}$ - $10^{-4}$	$10^{-6}$	Y	532	[6]
Au NP	16	1.6	CV/MG	$10^{-10}$ - $10^{-6}$	$10^{-10}$	Y	633	This work

## Reference

- [1] H. Xia, Y. Xiahou, P. Zhang, W. Ding and D. Wang, *Langmuir*, 2016, **32**, 5870–5880.
- [2] Y. Gao, T. You, N. Yang, C. Zhang and P. Yin, *Adv. Mater. Interfaces*, 2019, **6**, 1801966.
- [3] G. Shi, M. Wang, Y. Zhu, Y. Wang and H. Xu, *Appl. Surf. Sci.*, 2018, **459**, 802–811.
- [4] K. Wang, D.-W. Sun, H. Pu and Q. Wei, *Talanta*, 2021, **223**, 121782.
- [5] H. Tian, H. Li and Y. Fang, *ACS Appl. Mater. Interfaces*, 2019, **11**, 16207–16213.
- [6] H. Sun, H. Liu and Y. Wu, *Appl. Surf. Sci.*, 2017, **416**, 704–709.